Sensitive ultrawideband transparent PVDF-ITO ultrasound detector for optoacoustic microscopy

YU-HANG LIU[1,2], ALEXEY KURNIKOV[3], WEIYE LI[1,2], VYACHESLAV KAZAKOV[3], RUIQING NI[1,2], PAVEL SUBOCHEV[3], AND DANIEL RAZANSKY[1,2,*]

[1] *Institute for Biomedical Engineering and Institute of Pharmacology and Toxicology, Faculty of Medicine, University of Zurich, Zurich, Switzerland*
[2] *Institute for Biomedical Engineering, Department of Information Technology and Electrical Engineering, ETH Zurich, Zurich, Switzerland*
[3] *Institute of Applied Physics, Russian Academy of Sciences, Nizhny Novgorod, Russia*
**Corresponding author: daniel.razansky@uzh.ch*

Received XX Month XXXX; revised XX Month, XXXX; accepted XX Month XXXX; posted XX Month XXXX (Doc. ID XXXXX); published XX Month XXXX

A new type of ultrasound detection scheme based on a transparent polyvinylidene-fluoride indium-tin-oxide (PVDF-ITO) piezoelectric film has been developed for ultrawideband sensitive detection of optoacoustic (OA) signals down to noise equivalent pressure (NEP) of 8.4 Pa over an effective detection bandwidth extending beyond 30 MHz. The high signal-to-noise ratio and low noise performance were facilitated by employing a two-stage amplifier structure. The PVDF-ITO detector was directly mounted on a commercial high numerical aperture objective lens of a scanning optical-resolution OA microscopy system to obtain submicron resolution images without signal averaging, as demonstrated both in phantoms and *in vivo* measurements in mice. The transparent detection scheme further allows for the OA imaging modality to be easily integrated with other imaging techniques for diverse multi-modal biomedical imaging investigations.

Intravital optoacoustic (OA) microscopy enables the non-invasive monitoring of functional and molecular changes in hemodynamics and metabolism by detecting the optical absorption of tissue chromophores [1]. In particular, optical resolution optoacoustic microscopy (OR-OAM), integrating the merits of tightly focused optics with ultrasound (US) detection of the generated OA signals, has been used for a number of *in vivo* applications ranging from functional cerebrovascular evaluation [2], visualization of calvarian vascular patterns [3, 4] to longitudinal skin wound monitoring [5, 6]. OR-OAM systems are commonly equipped with either optical-acoustic combiners for conventional US detectors or ring-shaped US detectors allowing the light to be delivered through the central aperture [2, 4, 5, 7, 8]. However, the optical-acoustic combiners introduce undesirable wave-front distortions in both optical and acoustic paths, while ring-shaped US detectors provide limited acoustic sensitivity and signal-to-noise ratio (SNR) [1, 7].

In the past decade, diverse optically transparent US detectors have been proposed for OA applications. All-optical-based US detectors such as Fabry-Perot (FP) sensor [9] and micro-ring resonator (MRR) [10] are able to acquire US signals with a miniature element size, broadband frequency response and high sensitivity; however, additional sophisticated probe laser sources are required while the detection scheme further involves optical interferometry paths that are highly sensitive to temperature drifts and environmental vibrations [7]. Piezoelectric single crystals such as lithium niobite ($LiNbO_3$) or lead magnesium niobate-lead titanate (PMN-PT) have recently been proposed for manufacturing transparent US detectors [11-14]. The $LiNbO_3$-based detectors exhibit high optical transmission and high central frequency [11, 12]. Yet, due to acoustic impedance mismatches of the single crystal, the detection is limited to a relatively narrow frequency band thus compromising OA image quality [12]. The alternating current poled PMN-PT US detector can achieve high transparency and piezoelectric constant; nevertheless, this material is mainly suitable in the low frequency range due to its high electromechanical and dielectric properties [14], limiting its potential when it comes to high-resolution imaging applications.

By integrating indium-tin oxide (ITO) and chrome/copper materials as the electrodes, partially transparent US detectors using polyvinylidene fluoride (PVDF) have been developed for OA mesoscopy applications based on unfocused [15] and focused laser beams [16]. However, these studies yielded low detection sensitivity, thus extensive signal averaging was required to achieve adequate SNR levels [15]. In this work, we developed a sensitive ultrawideband transparent ultrasound detector (UTUD) based on a 48 μm PVDF film fully coated with ITO to serve as electrodes, equipped with a custom-made two-stage amplifier. The customized 3D-printed casing of UTUD allowed direct mounting on a commercial high numerical aperture (NA) objective lens of an OR-OAM system for acquiring submicron resolution images without the need for signal averaging.

A schematic diagram of UTUD is shown in Fig. 1. The ultrasonic sensing element of the detector was a planar PVDF-ITO piezo film fixed between two plastic washers on the conductive adhesive. The washers have an outer diameter of 5 mm, an inner diameter of 2.5 mm (corresponding to the effective sensing area of the detector), and thicknesses of 0.5 mm and 1 mm for the two layers (Fig. 1a). Signal and ground wires (attached to both sides of the piezo film) were connected to a matching broadband two-stage amplifier with dimensions of 13 mm × 7 mm × 2 mm. A resistor-capacitor (RC) circuit was installed between the amplification stages as a high pass filter to suppress the low-frequency (< 1 MHz) part of the input signal. The wire from the amplifier was then connected to a custom-made bias T diplexer, supplying 5 V direct current power for the UTUD. The sensing element and the amplifier were both hermetically placed in a custom-made plastic case

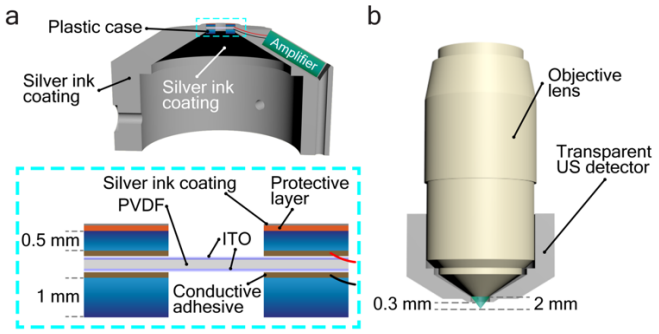

Fig. 1. Design and structure of the sensitive ultrawideband transparent ultrasound detector (UTUD). (a) Schematic of the transparent US detector with a double-sided ITO-coated PVDF film as the piezoelectric material. (b) 3D rendering of the UTUD mounted on a commercial objective lens, showing the approximate space (i.e., 0.3 mm) between the detector and target.

(Fig. 1b) made by a 3D printer (Shuffle, Phrozen, China). The geometry and dimensions of the outer housing were precisely designed based on the specification of the commercial objective lens. The UTUD housing was coated, both on its outer and inner surfaces, with silver ink (PolyK, USA) in order to shield it from external electrical noise. A thin coating of varnish was applied over the silver ink to prevent environmental damage to the shielding layer.

We first evaluated the main technical performance characteristics of the custom-made UTUD. The light transmission efficiency of a 48 μm thick PVDF film (PolyK, USA) was measured with and without ITO electrodes (Fig. 2a) over 400-1000 nm wavelength range. The transmission efficiency at 532 nm was only 57% thus an increased laser probing energy was needed to acquire OA signals. Yet, no observable damage was generated by the laser beam traversing the transparent piezo film. Sensitivity of the UTUD was measured by using a resonant piezoceramic emitter and compared with the performance of a calibrated 1 mm needle piezoelectric hydrophone (NH1000, Precision Acoustics, UK), which could be similarly placed in close vicinity to the objective lens for acquiring the generated OA signals. The diameter of the piezoceramic disk was 20 mm and the thickness was 1.8 mm, with a corresponding resonant frequency of the first harmonic of 1.194 MHz. For measuring the sensitivity, the emitter and both US detectors were placed parallel to each other spaced by 80 mm in a chamber filled with distilled water. The spacing was determined by the boundary of the near zone for the fundamental frequency of the emitter, where a uniform distribution of the ultrasonic wave was formed. A sinusoidal wave packet with the voltage ranging from 0.3 to 10 V was then applied to the emitter. Each packet consisted of at least 100 cycles and the interval between packets was 100 ms. Afterwards, the ultrasonic wave generated by the above emitter was recorded by the detectors and digitized by a two-channel analog-to-digital converter (ADC, AKIP-75244B, UK) with a resolution of 12 bits. The measurements were carried out at the first seven resonant frequencies of the emitter (i.e., 1.194, 3.774, 6.277, 8.758, 11.265, 13.766, 16.209 MHz). The resulting curves of sensitivity (μV/Pa) for both detectors were normalized to the gains and the excitation voltage of the emitter at each frequency (Fig. 2b). Note that our UTUD was calibrated based on both the above measurements and the sensitivity characteristic of NH1000 listed in the calibration report of the manufacturer.

To further assess the UTUD performance, we directly compared the OA signals and their corresponding spectra recorded by both types of US detectors from a thin black tape irradiated with focused pulsed laser radiation at 532 nm (Figs. 2c-d). Both OA signals were averaged 16

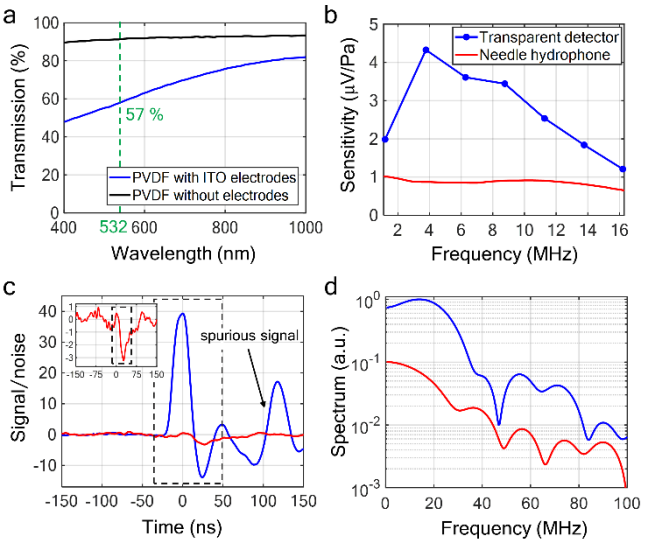

Fig. 2. Light transmission and US detection performance characteristics of the UTUD. (a) Light transmission efficiency of the piezo film. (b) Sensitivity of UTUD (2.5mm diameter aperture) versus 1mm diameter commercial needle hydrophone. (c) and (d) OA signal-to-noise ratios and their frequency spectra recorded by the UTUD (blue) and the needle hydrophone (red) from a thin black tape sample.

times and normalized to the gain and noise standard deviation for each of the detectors, resulting in a major SNR gain for the UTUD (Fig. 2c). The inset shows a zoomed OA waveform recorded by NH1000. Both recorded signals were further analyzed in the spectral domain (Fig. 2d). Note that the lower frequency portion was limited by the cutoff frequency of the built-in amplifiers, which was 1 MHz for the UTUD and 0.1 MHz for the NH1000 needle hydrophone. Table 1 lists the noise floor levels, averaged sensitivity, and corresponding noise equivalent pressure (NEP) for both detectors. The latter closely resembled the SNR differences of more than an order of magnitude between the detectors, as shown in Fig. 2c. Note that the NEP characterizes the noise level of the detector, expressed in units of pressure, and is defined as the ratio of the noise standard deviation to the averaged sensitivity value.

Table 1. Sensitivity comparison between two US detectors

	Noise floor (μV, rms)	Sensitivity (μV/Pa)	NEP (Pa)
UTUD	22.9	2.7	8.4
Needle hydrophone (NH1000)	67.8	0.8	85

In this study, an optical scanning OR-OAM system (Fig. 3a) was developed and integrated with the UTUD. A 532 nm nanosecond (ns) Q-switched diode-pumped solid-state laser (Onda 532, BrightSolutions, Italy) was used as the pumping source to generate OA signals at 10 kHz. An Iris (SM1D12D, Thorlabs, Germany) was placed after the laser output to adjust the pulsed beam shape, while a combination of half-wave plate (WPH05M-532, Thorlabs, Germany) and polarizing beam splitter (CCM1-PBS25-532- HP/M, Thorlabs, Germany) was employed to adjust the pulse energy. In addition, to compensate per-pulse laser energy fluctuation during post-processing, a small fraction of laser beam was sampled by a beam sampler (BSF10-A, Thorlabs, Germany) and detected by a photodetector (DET10A2, Thorlabs, Germany). Afterwards, the beam was directed into the light path of the custom-made 3-axis XYZ stage [17]. The laser beams were scanned by the 2-axis Galvo scanners (6215H, Cambridge Technology, USA), and

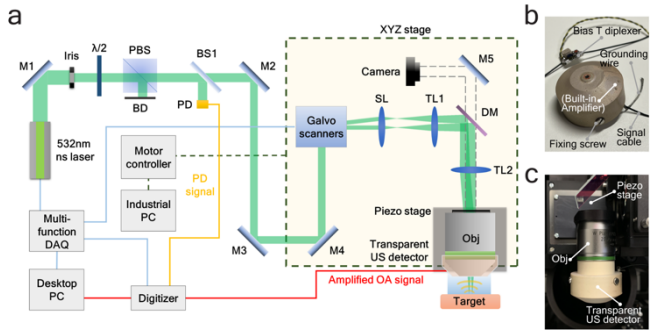

Fig. 3. The customized optical-resolution optoacoustic microscopy (OR-OAM) system (a) Schematic of the OR-OAM system integrated with the UTUD. (b) Photograph of the 3D-printed UTUD casing. (c) Photograph of the entire scanning head including the UTUD. M: mirror, λ/2: half-wave plate, PBS: polarizing beam splitter, BD: beam dump, BS: beam sampler, PD: photodiode, SL: scan lens, TL: tube lens, DM: dichroic mirror, Obj: objective lens.

sequentially passed through the scan lens (AC508-075-B, Thorlabs, Germany), tube lenses (AC508-300-B and AC508-400-B, Thorlabs, Germany) and the water immersion microscope objective lens (W-Plan Apochromat 20×/1.0 DIC, Zeiss, Germany) to focus beams onto the target. A piezo stage (P-628.1CD, Physik Instrumente, Germany) was employed to perform a fine Z-directional scan ranging from 800 µm. The generated OA signals were detected by the UTUD and acquired by a 2-channel, 250 MS/s, 16-bit digitizer (M4i.4420-x8, Spectrum, Germany) for further image reconstruction. The multi-function data acquisition (DAQ) cards (NI 6110 and NI 6229, National Instruments, USA) were used as the master controller to trigger the laser firing, Galvo scanning and data acquisition of the digitizer. A custom Matlab code (R2020b, The MathWorks, USA) was used to design the analog trigger patterns for Galvo scanners and reconstruct images based on the acquired OA signals.

The UTUD was equipped with a built-in two-stage amplifier in the customized 3D-printed casing. The first stage provided a high input impedance over a wide frequency band, which boosted the acquired electrical signal while maintaining minimal noise floor levels. The second stage directly provided a uniform 30-fold amplification up to 100 MHz. The two-stage amplifier arrangement can deliver signals to the digitizer with a higher gain, elevated SNR and minimal distortion. Note that the silver grounding wire connected from the amplifier (Fig. 3b) is needed to ground the metal housing of the objective lens with the UTUD to prevent noise from being coupled into the signal electrode/cable of the PVDF-ITO film. The customized casing of the UTUD also facilitates its direct mounting onto the commercial objective lens using the three fixation screws (Figs. 3b-c).

In vivo OA imaging performance was evaluated by imaging the ear vasculature in athymic nude mice (3 female mice, 12-week-old, Charles River, Germany). Mice were housed under a 12-hour-light/dark cycle, 20 - 24 °C temperature, and 50 - 70% humidity under specific pathogen-free conditions and received food and water *ad libitum*. Mouse maintenance and all animal experiments in this study were approved by the local veterinary authority (Kantonales Veterinäramt Zürich, Switzerland). Anesthesia was split into two phases with a mixture of isoflurane (Attane, USA; 3.5% for induction and 1.5% for maintenance) and oxygen/air (20/80%) for all experiments, while the oxygen saturation and CO_2 were monitored by PhysioSuite (Kent Scientific Corporation, USA). The mouse head was fixed by a head holder (SGM-4, Narishige, Japan) and its ear was placed on a customized 3D-printed board, and then a small amount of US gel was applied to ensure a good

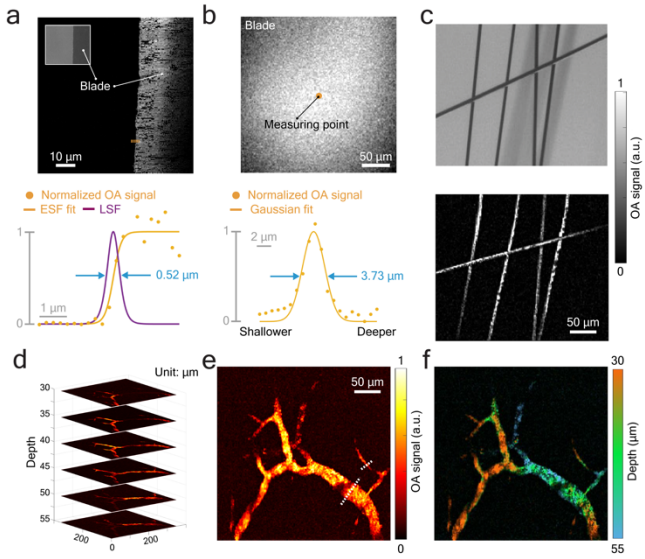

Fig. 4. Experimental OR-OAM imaging results based on the UTUD. (a) Lateral and (b) axial resolution determination of the OR-OAM system. (c) Microscope photo and OR-OAM image (maximum intensity projection along the depth axis) of 7 µm diameter carbon fibers. (d) Sequential *in vivo* OR-OAM mouse ear edge images acquired at different depths. (e) The corresponding maximum intensity projection (MIP) representation and (f) the color-encoded depth images.

acoustic coupling for OA imaging. A self-regulated heating pad at 36.8°C was employed to maintain normal mouse body temperature throughout the entire experimental procedure.

We determined the lateral resolution of the UTUD-based OR-OAM system by scanning the edge of a sharp surgical blade (Fig. 4a). The image was acquired with a step size of 0.26 µm over ~5 µm range in the lateral direction. The edge-spread function (ESF) was then determined as a logistic fit to OA data (Fig. 4a; orange dots: measured OA signals, solid orange line: ESF fit to OA data). Afterwards, the line-spread function (LSF) was obtained by numerical differentiation of the fitted ESF, and the resolution was measured as 0.52 µm based on the full-width-at-half-maximum (FWHM) of the normalized LSF (Fig. 4a; solid purple line) [17]. Due to the high NA of the objective lens, the effective axial resolution was dominated by the depth of field (DOF) of the optical focus [18]. A surgical blade was thus employed as the imaging target to measure the axial resolution of the OAM (Fig. 4b). A depth scanning with 1 µm step size and laser energy < 10 nJ was performed by using the piezo stage to acquire serial OA images. Normalized OA signal amplitudes at the measuring point of each depth were then processed to acquire their peak values. Based on the Gaussian fitting and FWHM calculation, the axial resolution was measured as 3.73 µm for the current imaging system (Fig. 4b), which is similar to the previously reported performance of OR-OAM systems employing high NA objective lens [18].

The imaging performance of the UTUD was first demonstrated in a phantom containing 7 µm diameter carbon fibers in 1% agarose (Merck, Germany). The brightfield photo (Fig. 4c; upper panel) shows the fiber arrangement with the corresponding OR-OAM image clearly discerning the fibers with high SNR (Fig. 4c; bottom panel). The latter image was acquired by a single plane scanning at ~14 nJ per pulse laser energy without employing signal averaging. Note that the carbon fibers at a deeper region (i.e., the thicker fibers shown in the photo) cannot be detected by our OR-OAM system, since the high NA objective lens

caused a largely unfocused beam and insufficient pulse energy outside the DOF of the optical objective for generating OA signals.

We further recorded *in vivo* images from the edge region of the mouse ear. For this, multiple cross-sections along the Z-direction were acquired with a spacing of 5 μm (Fig. 4d), corresponding to the characterized axial resolution and the short DOF. The individual slices clearly discerned the microvascular structures at different depths while the maximal intensity projection (MIP) images showed the entire vascular tree (Figs. 4e-f). The high sensitivity of the transparent detector is corroborated by the fact that both large (34.6 μm diameter) and small (4.3 μm diameter) capillaries (white dashed lines in Fig. 4d) are visible in the images without employing any signal averaging. The per pulse laser energy delivered was measured as ~150 nJ. The ns laser was tightly focused on the blood vessels within the dermis layer located 20 - 30 μm underneath the epidermis layer (i.e., the skin surface) [19]. Thus, the light fluence on the ear surface was 7.34 mJ/cm^2, which is within the American National Standards Institute (ANSI) laser safety limits. We also observed no bleeding or other tissue damage during the *in vivo* experiments.

Compared to other piezoelectric single crystal materials [11, 12, 14], PVDF was selected as the US sensing material due to its characteristically low acoustic impedance and broadband acoustic response [16], which also simplified the US detector manufacture by avoiding matching and damping layers. PVDF is known to exhibit a relatively low electromechanical coupling coefficient compared to other piezoelectric materials. We thus employed the two-stage amplifier design to further elevate the sensitivity while maintaining low NEP (Table 1). Note that the current ITO coating material used for the electrodes is not an optimal choice for fabricating the transparent US detector, since the high sheet resistance of ITO limits conductivity thus increasing the signal loss [16]. Therefore, alternative materials like silver nanowires would be a better choice, providing both good light transmittance and low sheet resistance [12].

In order to target micrometer-sized structures, e.g., microcapillaries, we designed the OR-OAM system with a commercial high NA objective lens attaining excellent lateral resolution. Remarkably, the limited size of the UTUD allows the detector to be directly placed under the objective lens even with a short focusing distance (e.g., 2 mm) without inducing wave-front distortions. This facilitates detection of high-frequency components in the generated OA signals, which are otherwise heavily attenuated after traveling over longer distances [1]. In addition, the design of our UTUD also maximizes the flexibility for choosing commercial objective lenses with diverse configurations to either increase the field of view (FOV) or further improve the lateral resolution based on the needs of particular biological applications.

The presence of a spurious signal (Fig. 2c) is associated with the absence of a damping layer for the piezoelectric film. Due to a large difference in acoustic impedances at the piezo film-air interface, a US reflection was produced and recorded by the detector. However, the observed reverberations did not adversely affect the overall quality of the phantom and *in vivo* images, since only the maximum signal intensities in each waveform were used for reconstructing the OR-OAM images. It is still possible to eliminate the parasitic component of the signal by employing an optically transparent material with an acoustic impedance close to that of the damping layer of the piezo film, such as transparent photopolymer resin or degassed nonconductive epoxy [12].

In summary, we developed a sensitive transparent ultrawideband US detector for acquiring OR-OAM images with submicron resolution. The simple design of UTUD allows for a potential combination with diverse objective lenses and thus an easy integration with other imaging modalities sharing the same optics (e.g., optical coherence tomography (OCT) [12] and two-photon microscopy (2PM) techniques [18]), thus providing complementary information within the same FOV. Future research will optimize electrode materials to enhance conductivity, explore defocusing schemes to increase sensitivity, develop multi-modal combinations with optical microscopy, and apply the method for a broad range of biological applications such as imaging of brain activity.

Funding. YHL acknowledges support from the UZH Postdoc Grant. The development of UTUD was supported by the Centre of Excellence "Center of Photonics" funded by the Ministry of Science and High Education of the Russian Federation, agreement No. 075-15-2020-906.

Acknowledgments. We thank Dr. H. Estrada for his help with the ultrasound simulations, Dr. U. Hofmann for electronic test of the UTUD, M. Prudnikov and V. Vorobyev for technical assistance with manufacturing the UTUD.

Disclosures. The authors declare no conflicts of interest.

Data availability. The data that support the findings of this study are available from the corresponding author upon reasonable request.

REFERENCES

1. S. M. Maswadi, B. L. Ibey, C. C. Roth, D. A. Tsyboulski, H. T. Beier, R. D. Glickman, and A. A. Oraevsky, Photoacoustics **4**, 91-101 (2016).
2. J. Yao, L. Wang, J. M. Yang, K. I. Maslov, T. T. Wong, L. Li, C. H. Huang, J. Zou, and L. V. Wang, Nat Methods **12**, 407-410 (2015).
3. W. Li, Y. H. Liu, H. Estrada, J. Rebling, M. Reiss, S. Galli, C. Nombela-Arrieta, and D. Razansky, J Bone Miner Res (2022).
4. H. Estrada, J. Rebling, U. Hofmann, and D. Razansky, Photoacoustics **19**, 100178 (2020).
5. Y. H. Liu, L. M. Brunner, J. Rebling, M. Ben-Yehuda Greenwald, S. Werner, M. Detmar, and D. Razansky, Theranostics **12**, 558-573 (2022).
6. J. Rebling, M. Ben-Yehuda Greenwald, M. Wietecha, S. Werner, and D. Razansky, Adv Sci (Weinh) **8**, 2004226 (2021).
7. D. Ren, Y. Sun, J. Shi, and R. Chen, Photonics **8**, 324 (2021).
8. Y. Liang, L. Jin, B. O. Guan, and L. Wang, Opt Lett **42**, 1452-1455 (2017).
9. E. Zhang, J. Laufer, and P. Beard, Appl Opt **47**, 561-577 (2008).
10. B. Dong, H. Li, Z. Zhang, K. Zhang, S. Chen, C. Sun, and H. F. Zhang, Optica **2**, 169-176 (2015).
11. R. Chen, Y. He, J. Shi, C. Yung, J. Hwang, L. V. Wang, and Q. Zhou, IEEE Trans Ultrason Ferroelectr Freq Control **67**, 1848-1853 (2020).
12. J. Park, B. Park, T. Y. Kim, S. Jung, W. J. Choi, J. Ahn, D. H. Yoon, J. Kim, S. Jeon, D. Lee, U. Yong, J. Jang, W. J. Kim, H. K. Kim, U. Jeong, H. H. Kim, and C. Kim, Proc Natl Acad Sci U S A **118** (2021).
13. C. Qiu, B. Wang, N. Zhang, S. Zhang, J. Liu, D. Walker, Y. Wang, H. Tian, T. R. Shrout, Z. Xu, L. Q. Chen, and F. Li, Nature **577**, 350-354 (2020).
14. B. Park, M. Han, J. Park, T. Kim, H. Ryu, Y. Seo, W. J. Kim, H. H. Kim, and C. Kim, Photoacoustics **23**, 100290 (2021).
15. C. Fang, and J. Zou, Opt Lett **46**, 3280-3283 (2021).
16. C. Fang, H. Hu, and J. Zou, IEEE Sensors Journal **20**, 2313-2319 (2020).
17. J. M. Mayrhofer, F. Haiss, D. Haenni, S. Weber, M. Zuend, M. J. Barrett, K. D. Ferrari, P. Maechler, A. S. Saab, J. L. Stobart, M. T. Wyss, H. Johannssen, H. Osswald, L. M. Palmer, V. Revol, C. D. Schuh, C. Urban, A. Hall, M. E. Larkum, E. Rutz-Innerhofer, H. U. Zeilhofer, U. Ziegler, and B. Weber, Biomed Opt Express **6**, 4228-4237 (2015).
18. W. Song, Q. Xu, Y. Zhang, Y. Zhan, W. Zheng, and L. Song, Sci Rep **6**, 32240 (2016).
19. W. Song, W. Zheng, R. Liu, R. Lin, H. Huang, X. Gong, S. Yang, R. Zhang, and L. Song, Biomed Opt Express **5**, 4235-4241 (2014).

REFERENCES with titles

[1] S. M. Maswadi et al., "All-optical optoacoustic microscopy based on probe beam deflection technique," Photoacoustics, vol. 4, no. 3, pp. 91-101, Sep 2016, doi: 10.1016/j.pacs.2016.02.001.

[2] J. Yao et al., "High-speed label-free functional photoacoustic microscopy of mouse brain in action," Nat Methods, vol. 12, no. 5, pp. 407-10, May 2015, doi: 10.1038/nmeth.3336.

[3] W. Li et al., "Tracking Strain-Specific Morphogenesis and Angiogenesis of Murine Calvaria with Large-Scale Optoacoustic and Ultrasound Microscopy," J Bone Miner Res, Feb 27 2022, doi: 10.1002/jbmr.4533.

[4] H. Estrada, J. Rebling, U. Hofmann, and D. Razansky, "Discerning calvarian microvascular networks by combined optoacoustic ultrasound microscopy," Photoacoustics, vol. 19, p. 100178, Sep 2020, doi: 10.1016/j.pacs.2020.100178.

[5] Y. H. Liu et al., "Non-invasive longitudinal imaging of VEGF-induced microvascular alterations in skin wounds," Theranostics, vol. 12, no. 2, pp. 558-573, 2022, doi: 10.7150/thno.65287.

[6] J. Rebling, M. Ben-Yehuda Greenwald, M. Wietecha, S. Werner, and D. Razansky, "Long-Term Imaging of Wound Angiogenesis with Large Scale Optoacoustic Microscopy," Adv Sci (Weinh), vol. 8, no. 13, p. 2004226, Jul 2021, doi: 10.1002/advs.202004226.

[7] D. Ren, Y. Sun, J. Shi, and R. Chen, "A Review of Transparent Sensors for Photoacoustic Imaging Applications," Photonics, vol. 8, no. 8, p. 324, 2021. [Online]. Available: https://www.mdpi.com/2304-6732/8/8/324.

[8] Y. Liang, L. Jin, B. O. Guan, and L. Wang, "2 MHz multi-wavelength pulsed laser for functional photoacoustic microscopy," Opt Lett, vol. 42, no. 7, pp. 1452-1455, Apr 1 2017, doi: 10.1364/OL.42.001452.

[9] E. Zhang, J. Laufer, and P. Beard, "Backward-mode multiwavelength photoacoustic scanner using a planar Fabry-Perot polymer film ultrasound sensor for high-resolution three-dimensional imaging of biological tissues," Appl Opt, vol. 47, no. 4, pp. 561-77, Feb 1 2008, doi: 10.1364/ao.47.000561.

[10] B. Dong et al., "Isometric multimodal photoacoustic microscopy based on optically transparent micro-ring ultrasonic detection," Optica, vol. 2, no. 2, pp. 169-176, 2015, doi: 10.1364/OPTICA.2.000169.

[11] R. Chen et al., "Transparent High-Frequency Ultrasonic Transducer for Photoacoustic Microscopy Application," IEEE Trans Ultrason Ferroelectr Freq Control, vol. 67, no. 9, pp. 1848-1853, Sep 2020, doi: 10.1109/TUFFC.2020.2985369.

[12] J. Park et al., "Quadruple ultrasound, photoacoustic, optical coherence, and fluorescence fusion imaging with a transparent ultrasound transducer," Proc Natl Acad Sci U S A, vol. 118, no. 11, Mar 16 2021, doi: 10.1073/pnas.1920879118.

[13] C. Qiu et al., "Transparent ferroelectric crystals with ultrahigh piezoelectricity," Nature, vol. 577, no. 7790, pp. 350-354, Jan 2020, doi: 10.1038/s41586-019-1891-y.

[14] B. Park et al., "A photoacoustic finder fully integrated with a solid-state dye laser and transparent ultrasound transducer," Photoacoustics, vol. 23, p. 100290, Sep 2021, doi: 10.1016/j.pacs.2021.100290.

[15] C. Fang and J. Zou, "Acoustic-resolution photoacoustic microscopy based on an optically transparent focused transducer with a high numerical aperture," Opt Lett, vol. 46, no. 13, pp. 3280-3283, Jul 1 2021, doi: 10.1364/OL.423287.

[16] C. Fang, H. Hu, and J. Zou, "A Focused Optically Transparent PVDF Transducer for Photoacoustic Microscopy," IEEE Sensors Journal, vol. 20, no. 5, pp. 2313-2319, 2020, doi: 10.1109/JSEN.2019.2952971.

[17] J. M. Mayrhofer et al., "Design and performance of an ultra-flexible two-photon microscope for in vivo research," Biomed Opt Express, vol. 6, no. 11, pp. 4228-37, Nov 1 2015, doi: 10.1364/BOE.6.004228.

[18] W. Song, Q. Xu, Y. Zhang, Y. Zhan, W. Zheng, and L. Song, "Fully integrated reflection-mode photoacoustic, two-photon, and second harmonic generation microscopy in vivo," Sci Rep, vol. 6, p. 32240, Aug 31 2016, doi: 10.1038/srep32240.

[19] W. Song et al., "Reflection-mode in vivo photoacoustic microscopy with subwavelength lateral resolution," Biomed Opt Express, vol. 5, no. 12, pp. 4235-41, Dec 1 2014, doi: 10.1364/BOE.5.004235.

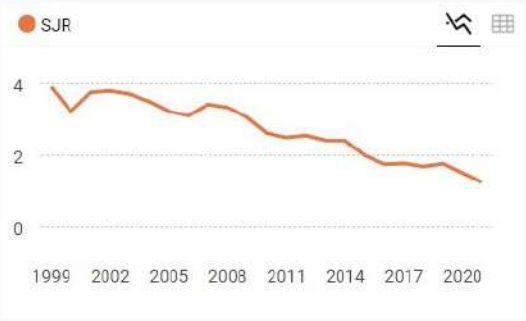

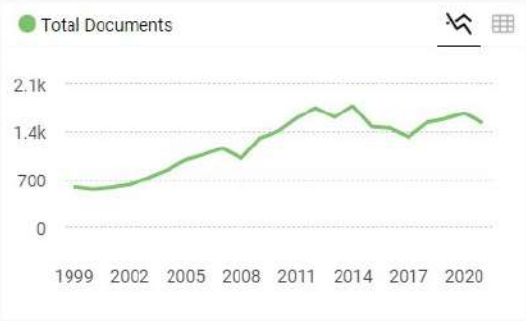

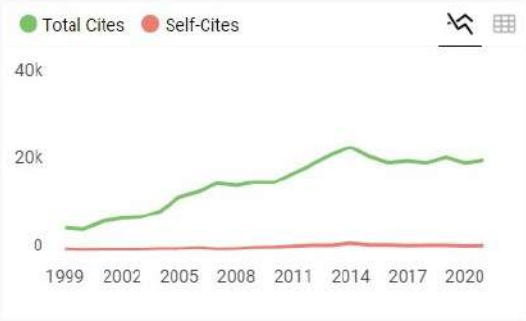

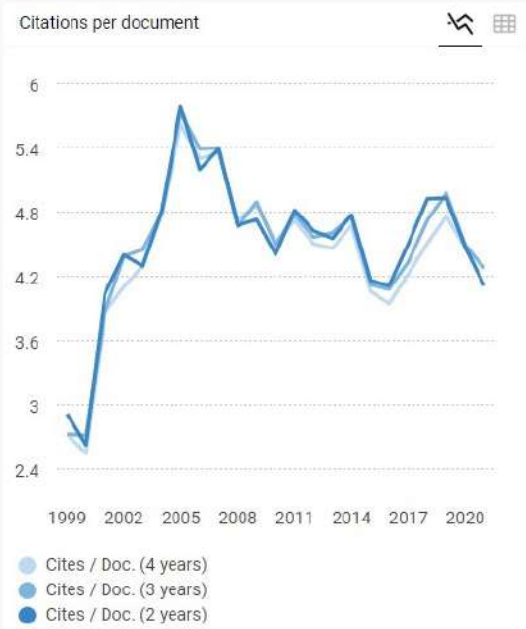

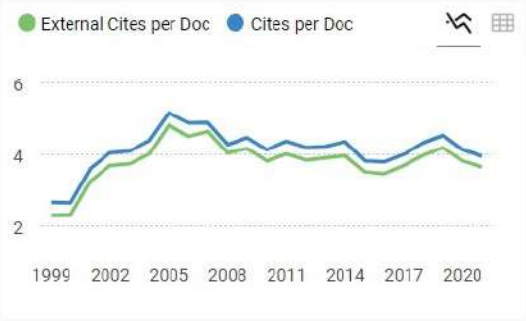

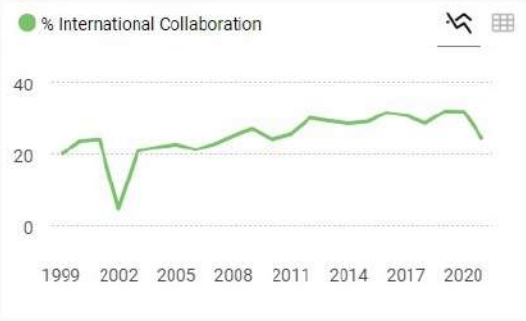

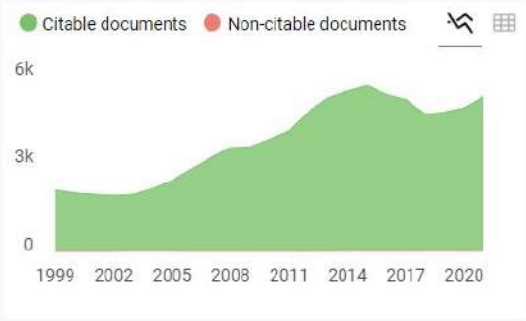

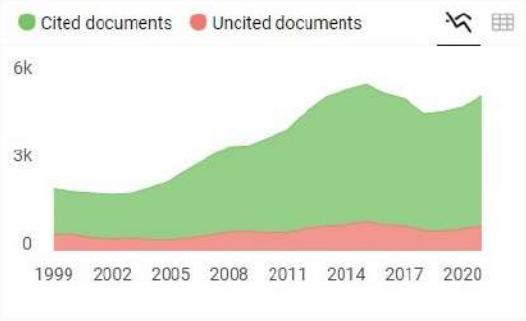

← Show this widget in your own website

Just copy the code below and paste within your html code:

```
<a href="https://www.scimag
```

SCImago Graphica

Explore, visually communicate and make sense of data with our **new data visualization tool**.